Int.J.Curr.Microbiol.App.Sci (2020) *9*(10): 2327-2338

International Journal of Current Microbiology and Applied Sciences
ISSN: 2319-7706 **Volume 9 Number 10 (2020)**
Journal homepage: http://www.ijcmas.com

Original Research Article https://doi.org/10.20546/ijcmas.2020.910.280

Optimization of Spur Gear Design with Different Root Fillet Profile

Yatih Nupur*

Vehicle Design and Integration, Knowledge Management Centre, Escorts Limited, India

**Corresponding author*

Keywords

Root fillet, Spur gear, Contact stress, pitting, CATIA V5, ANSYS, Photo elastic method

Article Info

Accepted:
17 September 2020
Available Online:
10 October 2020

A B S T R A C T

Failure and pitting of teeth of gear affects transmission error. So, aim of this study was to define optimal tooth modifications introduced by performing static contact and deformation analysis, while trying to design spur gears to resist failure and pitting of the teeth. Behaviour of unusual contact between flywheel ring gear and starter motor pinion was analysed and optimized root fillet was introduced in spur gear. Starter pinion was analysed in ANSYS for deformation and maximum contact stress which causes pitting. Experimental Analysis was done using photo elastic method on photoelastic apparatus and compares the FEM result with experimental result. For this work parametric modeling was done using CATIA V5 and for analysis ANSYS workbench was used.

Introduction

In almost every mechanism, gears are extensively used machine parts to transmit power from one shaft to other with or without change of speed or direction. Gear is the rotating machine element that can transmit the power, motion and torque. The spur gear is the simplest type of gear having teeth projecting radially. Generally, the efficiency of gear is nearly 98%. They are usually employed to achieve constant drive ratio(1). The formal methods for design of gear use ISO (International Organization for Standardization) or AGMA (American Gear Manufacturers Association standards) (2). The need for better and efficient power transmission has increased the demand for effective gear design systems. The significance of toothed gears for power and motion transmission is proved by the fact that they are the machine elements mostly used in a large range of engineering applications. Their mechanical behaviour is critical for the performance of the assembly in terms of reliability and fatigue endurance. A key factor of their behaviour is the design of the gear tooth towards optimized stress distribution.

Contact stress refers to the localized stresses that develop as two curved surfaces come in contact and deform slightly under the imposed loads. Also due to contact stresses wear takes place at gear tooth (3). Studies done by Rahate al. (4) on contact stress analysis of steel gear and composite gear using Hertz equation and by Finite Element Analysis using Ansys 16.0 Workbench. Also experimental stresses are calculated using Photo-Stress Method. Naik *et al.,* (5) analysed the bending stresses occur on the gear tooth profile when subjected to loading condition with the help of FEM and Photo-elastic technique. Rameshkumar *et al.,* (6) carried out static finite element analysis for NCR and HCR gears with fixed module, centre distance and gear ratio. Here the increasing contact ratio is obtained by increasing the addendum factor from 1.0 to1.25 m. Hence a contact ratio of more than 2.0 was achieved for the same number of teeth.

Patil *et al.,* (7) reported the contact stresses among the Spur gear pair and Helical gear pair, under static condition by using 3D finite element model. For the spur gear pair, the increase in contact stress with the increase in coefficient of friction was about 10%.

A better control during the last decades of the quality of the materials, the surface finishing and the heat-treatment process has prevented the two main and classical modes of fatigue damages for gears: (i) tooth bending root fatigue and (ii) flank surface contact fatigue. These two classical damage modes are well established and addressed in the international standards such as ISO 6336 part 2 and 3 (8-9). However, up to now there are very less research work are available to predict the optimum gear life through modification of root fillet profile. The proposed work focuses on the experimental investigation of the stress field around a gear tooth due to unusual contact between flywheel ring gear and starter motor pinion with objective

1. To predict stress and deformation generated on pinion in order to expose the behavior of pinion when comes in contact with ring gear.
2. To analyze the effect of tooth modification from root on stresses generated, deformation of tooth.
3. To perform the photo elastic experimentation analysis in transmission type polariscope along with the finite elemental analysis in Ansys.

Materials and Methods

Properties of material

Compressive Yield Strength	**250MPa**
Tensile Yield Strength	250MPa
Tensile Ultimate Strength	460MPa
Young's Modulus	200GPa
Poisson's Ratio	0.3
Density	7850 kg m3
Reference Temperature	22^0C

Working geometry

Fine meshing is applied to pinion for obtaining more precise results i.e. contours after meshing number of nodes and elements are 11221 and 10744 respectively, meshing of the geometry shown in Fig. 1 and 2.

Finite element analysis of system

Pre-processing and boundary condition

The model is imported to ANSYS Design Modular for CATIA V5R18, this model consists of 126 teeth Ring gear and 8 teeth pinion. For the ease of working and reducing analysis time the number of tooth on ring gear are reduced to 4 tooth only as shown below

Load and boundary condition of connecting rod

In case of FEA the pinion is added as a contact body and ring gear as a target body shown in Fig-3. The type of contact used is frictionless no separation type, shown in Fig-4. The no separation contact is added between two tooth in contact.

The revolution of pinion is considered for "RZ" direction while ring gear is kept at constant position shown in Fig-5. The ring gear body is considered as a fix support, moment of "27852 N-mm" is added along Z-Axis i.e. it will rotate along Z direction. The specification of particular starter motor is 1200RPM and the rated power output is 3.5KW. The moment applied is shown in Fig-6.

Experimental analysis

Two-dimensional Photo elasticity

The foregoing is a rather general description of the formation of photoelastic patterns. It applies equally well to two-dimensional and three-dimensional photoelasticity and to the method of photoelastic coatings. Now, let us restrict the discussion to plane-stress systems, so that the basis of photoelasticity can be developed without needless complications. A plane-stress problem is approached when the thickness (lateral dimension) of the prototype and the model is small in relation to dimensions in the plane, and the applied forces act in the plane at mid thickness. For such a system, we are concerned with stresses acting parallel to the plane of the model only, for all other stress components are zero.

Mentally remove any small element, oriented such that the faces of the element are principal planes. The surfaces of the model are automatically principal planes (for no shear stress acts on these surfaces). Define the orientation of principal planes by the angle ϕ, and letσ1alwaysrepresent the algebraically larger of the two principal stresses, such that (σ1-σ2) is always positive. The objective now is to show how stresses and stress directions are derived from photoelastic patterns.

For two dimensional analysis, the most sufficient dimensionless ratio is the ratio ($\sigma hl/p$) Where $\sigma$is the stress at any point, 'P' is the applied load, h is the thickness and 'l' is the typical length dimension. If subscripts 'p' and 'm' refer to the prototype and model respectively. Scale relation as follows,

$$\frac{\sigma m}{Pm} = \frac{\sigma p}{Pp} \times \frac{hp}{hm} \times \frac{lp}{lm}$$

The values of stresses and loads in prototype i.e. $'\sigma p'$and 'Pp' are taken from theoretical analysis of gear. The value of model thickness 20 mm and prototype thickness 8 mm are used for polariscope calculations.

Technical data (Light source)

a) lamp box with white diffuser
b) For white light: -
1 fluorescent tube
2 incandescent lamps, candle bulb, matt inner E14, 235V, 25W
c) For mono chromatic light (color yellow)
1 sodium vapor lamp SOX 35, 35W
d) Filter, enclosed in glass, diameter: d=425mm
e) - 2 polarization filters (dark olive)
f) - 2 quarter wave filters (colorless)
g) Frame W×H : 600×750mm

Stress optic law

According to Maxwell theory,

$(n_1 - n_2) = K (\sigma_1 - \sigma_2)$…… (a)

Where,
n_1 and n_2 are indices of refraction along directions of principle stress σ_1 and σ_2 and K is constant called as Stress optic coefficient.

The polarized light vector splits into two components along axis ofσ_1 and σ_2 propagates with different velocities say V1 and V2 required for light vector to come out of thickness h will be,

$t_1 = h / V_1$ and $t_2 = h / V_2$

Relative retardation in time will be

$(t_1 - t_2) = h(1/ V1 – 1/ V2)$

If C is velocity of light in air, in the relative distance between two components will be,

$$\delta = h(t1 - t2) = h\ (C/\ V1 – C/\ V2)$$

But,
$C/\ V1 = n_1$ and $C/\ V2 = n_2$
$\delta = h(n1 - n2)$
$\delta = h\ .K\ (\sigma_1 - \sigma_2)$…….. from (a)

For linear retardation of one wavelength λ, the angular retardation is 2λ radians, hence the angular retardation$\alpha$for linear retardationδwill be,

$\alpha = \delta . 2\pi / \lambda$
$\alpha = h.K / \lambda \times 2\pi(\sigma_1 - \sigma_2)$
$\sigma_1 - \sigma_2 = \frac{\alpha}{2\pi} \times \frac{\lambda}{K} \times \frac{1}{h}$
$\sigma_1 - \sigma_2 = \frac{N.f\sigma}{h}$

Where,
$N = \frac{\alpha}{2\pi}$
$f^{\sigma} = \frac{\lambda}{K}$Material fringe value
h = model thickness in mm

The above equation gives practical expression of stress optic law which is used for determining the stress difference (σ_1-σ_2). Material fringe value can be find out by calibration of photoelastic material, model thickness is known and fringe order is find out by experimentally using polariscope.

Results and Discussion

FEA results

For the predictions of maximum deformation and equivalent stress generated, the system of gears is analysed by modifying it with different cases of varying fillet radius. The modification range is from 0.5mm to 1.5 mm at an interval of 0.25 mm, results of analysis parameters is compared with the results obtain from working geometry.

In this determining the stress values from the observed fringe order. The fringe order observed from the experimentation is as shown in Table 1 (Fig. 1–24).

Determining material fringe value

As we know;

$f^{\sigma} = 8p / \pi DN$

where,

N = Exact fringe order
P = Load applied
D = Diameter of Disc
Putting Values in equation above
$f^{\sigma} = 8 \times 101.936 / \pi \times 86 \times 0.42$
$f^{\sigma} = 7.186$

The material fringe value (f^{σ}) is important for calculating stress and it common for all calculations.

Determining stress values for working geometry

Determining stress values for geometry with root fillet of 0.25mm

By stress optics law,

$$\sigma_1-\sigma_2 = \frac{N.f\sigma}{h}$$

$$\sigma_1-\sigma_2 = \frac{0.62 \times 7.186}{8}$$

Put σ_2 =0

$\sigma_1 = \sigma_p$= 0.5569 N/mm^2

P= Prototype

M= Model

$$\frac{\sigma m}{Pm} = \frac{\sigma p}{Pp} \times \frac{hp}{hm} \times \frac{lp}{lm}$$

After rearrange the equation above, we get;

$$\sigma m = \sigma p \times \frac{Pm}{Pp} \times \frac{hp}{hm} \times \frac{lp}{lm}$$

$$\sigma m = 0.5569 \times \frac{27852}{101.936} \times \frac{8}{20} \times \frac{21}{12}$$

$$\sigma m = 106.51\ MPa$$

Determining stress values for geometry with root fillet of 0.5mm

By stress optics law,

$$\sigma_1-\sigma_2 = \frac{N.f\sigma}{h}$$

$$\sigma_1-\sigma_2 = \frac{0.89 \times 7.186}{8}$$

Put σ_2 =0

$\sigma_1 = \sigma_p$= 0.801 N/mm^2

P= Prototype

M= Model

$$\sigma m = \sigma p \times \frac{Pm}{Pp} \times \frac{hp}{hm} \times \frac{lp}{lm}$$

$$\sigma m = 0.801 \times \frac{27852}{101.936} \times \frac{8}{20} \times \frac{21}{12}$$

$$\sigma m = 153.199\ MPa$$

Table.1 Exact fringe order for six cases

Sr. No	Cases	Exact Fringe Order
1.	I.	0.62
2.	II.	0.89
3.	III.	1.05
4.	IV.	1.02
5.	V.	0.96
6.	VI.	0.87

Table.2 Comparison of stresses obtained from FEA and ESA

Sr. No.	Added Root Fillet (mm)	Stress (MPa)			Deformation
		FEA	ESA	% Error	
1	Working geometry	104.53	106.51	1.86	0.0102
2	0.5	150.51	153.199	1.76	0.0097
3	0.75	176.54	179.78	1.80	0.0099
4	1.0	170.77	175.19	2.25	0.0096
5	1.25	160.91	166.39	3.29	0.0091
6	1.5	140.1	143.5	2.37	0.0079

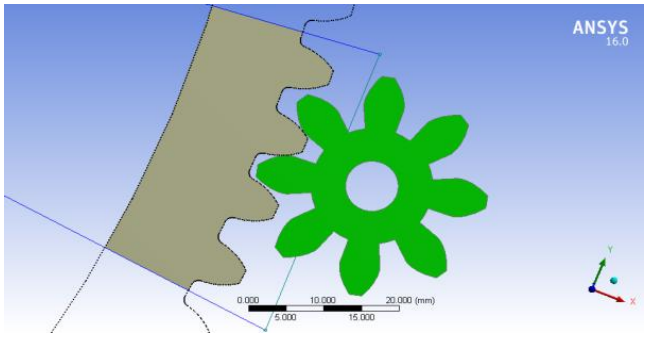

Fig.1 Working geometry

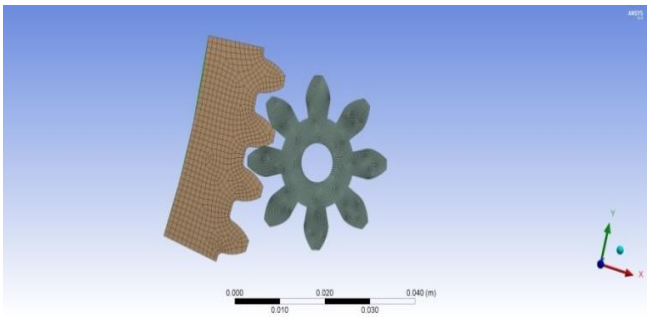

Fig.2 Meshing

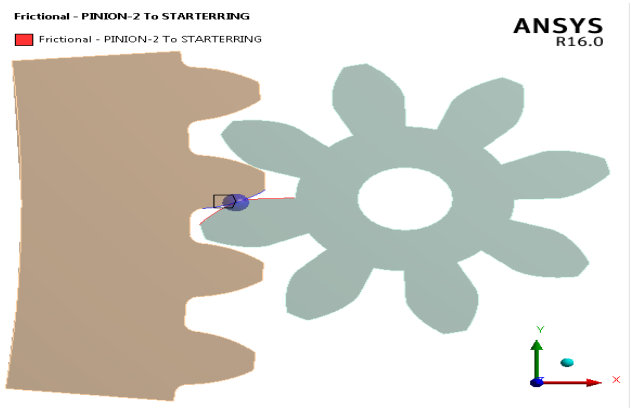

Fig.3 Contact between gear teeth

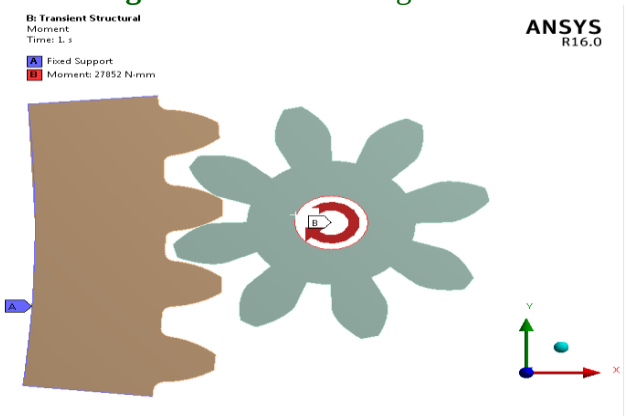

Fig.4 Type of support

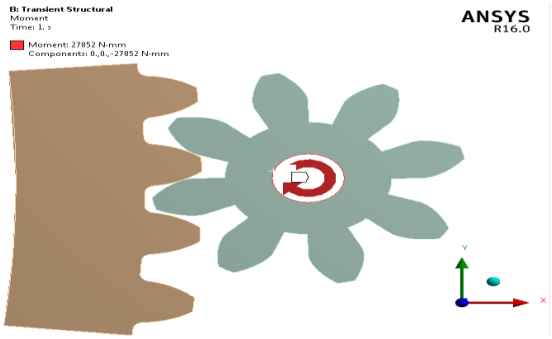

Fig.5 Direction of revolution of pinion

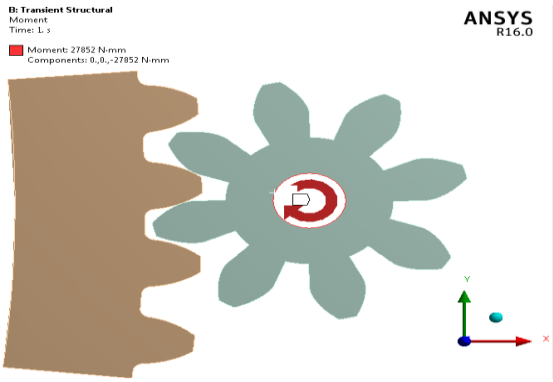

Fig.6 Moment applied to pinion

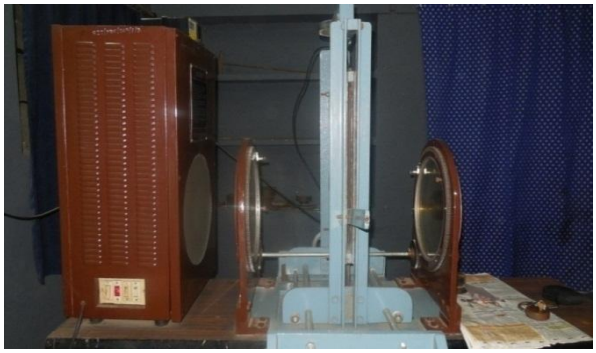

Fig.7 Experimental Setup

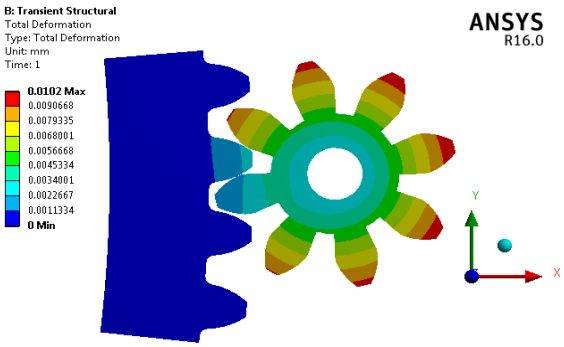

Fig.8 Deformation in working geometry

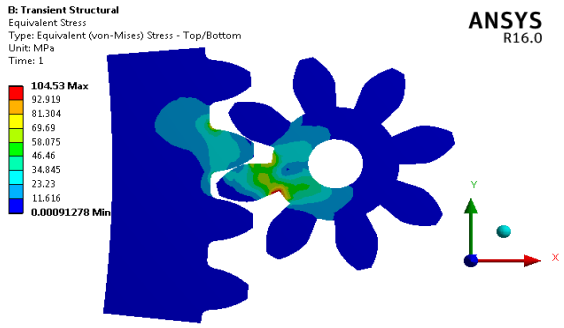

Fig.9 Stresses in working geometry

Deformation and Stresses in modified geometry of 0.5 mm root fillet

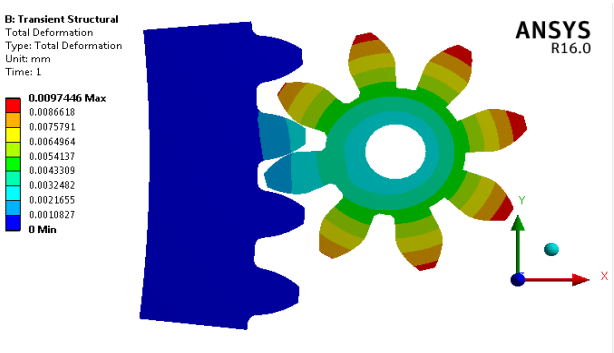

Fig.10 Deformation in modified geometry of 0.5 mm root fillet

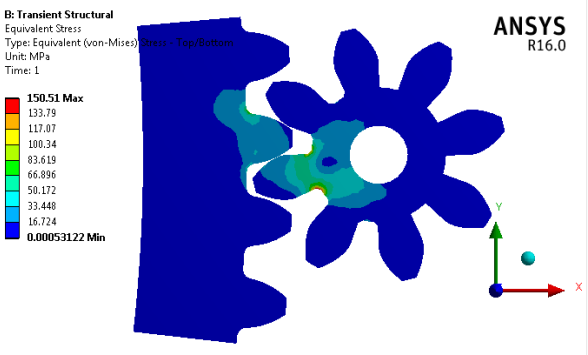

Fig.11 Stresses in modified geometry of 0.5 mm root fillet

Deformation and Stresses in modified geometry of 0.75 mm root fillet

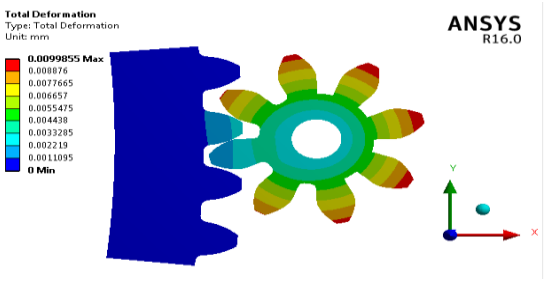

Fig.12 Deformation in modified geometry of 0.75 mm root fillet

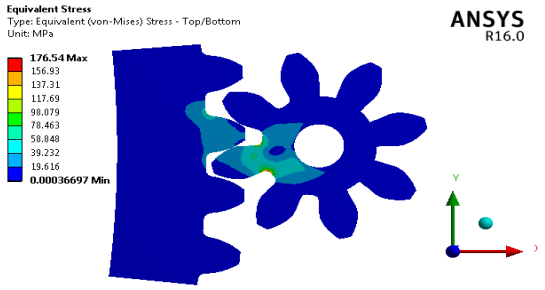

Fig.13 Stresses in modified geometry of 0.75 mm root fillet

Deformation and Stresses in modified geometry of 1.0 mm root fillet

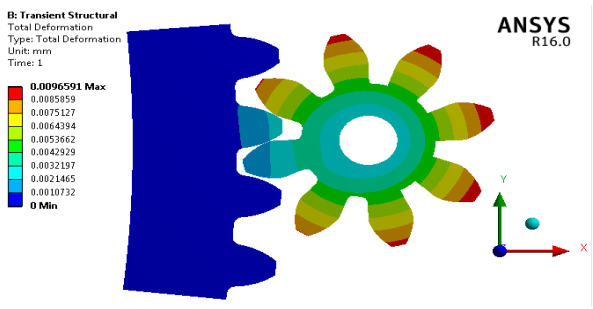

Fig.14 Deformation in modified geometry of 1.0 mm root fillet

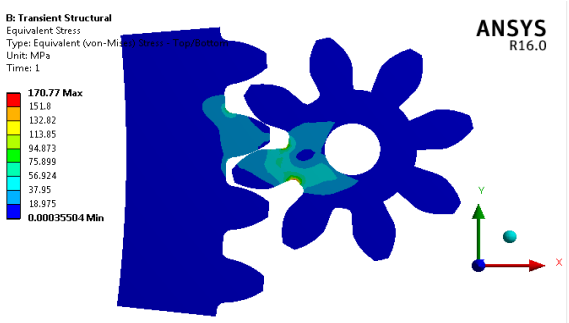

Fig.15 Stresses in modified geometry of 1.0 mm root fillet

Deformation and Stresses in modified geometry of 1.25 mm root fillet

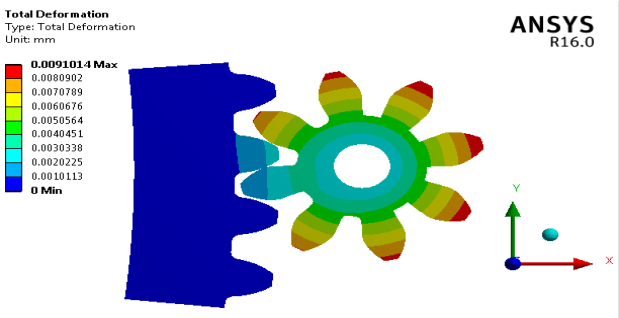

Fig.16 Deformation in modified geometry of 1.25 mm root fillet

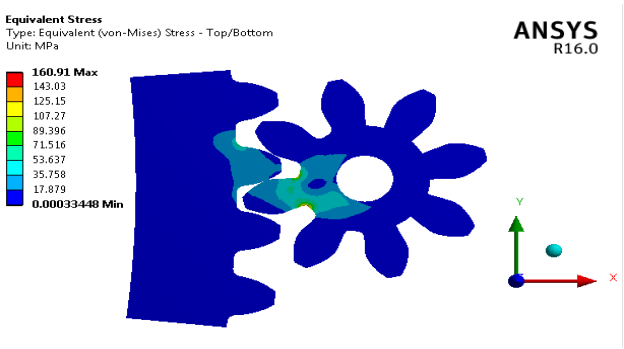

Fig.17 Stresses in modified geometry of 1.25 mm root fillet

Deformation and Stresses in modified geometry of 1.5 mm root fillet

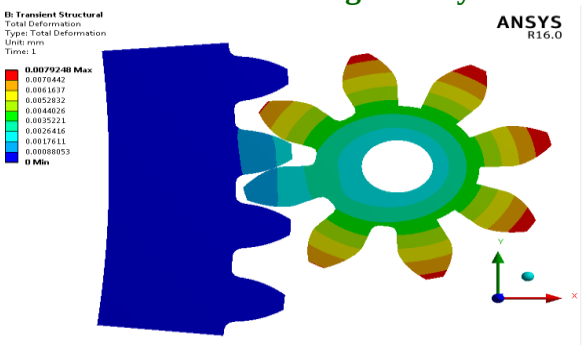

Fig.18 Deformation in modified geometry of 1.5 mm root fillet

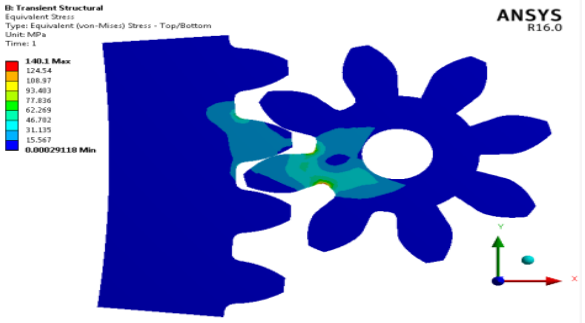

Fig.19 Stresses in modified geometry of 1.5 mm root fillet

Experimentation Results

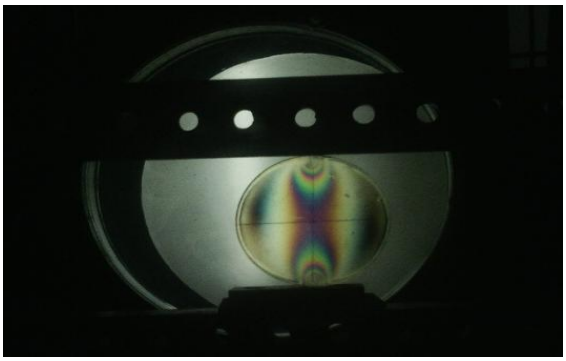

Fig.20 Obtaining value of "$f\sigma$" material Fringe value

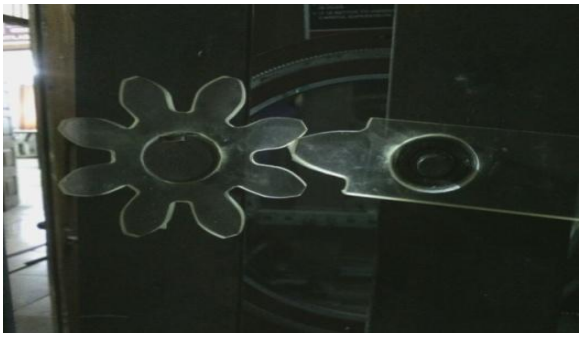

Fig.21 Loading of assembly on polariscope

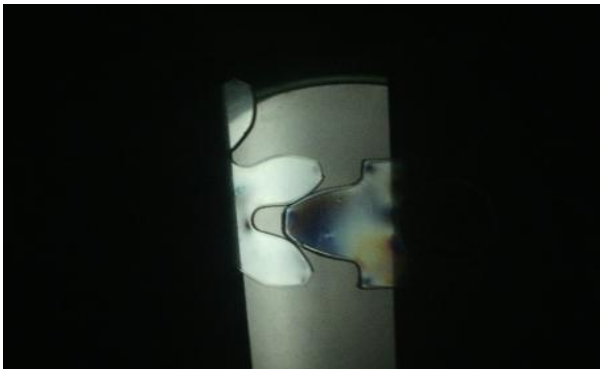

Fig.22 Photoelastic gear at no load condition

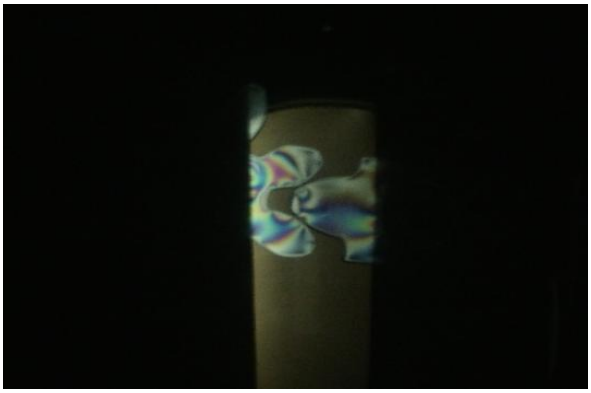

Fig.23 Fringe pattern

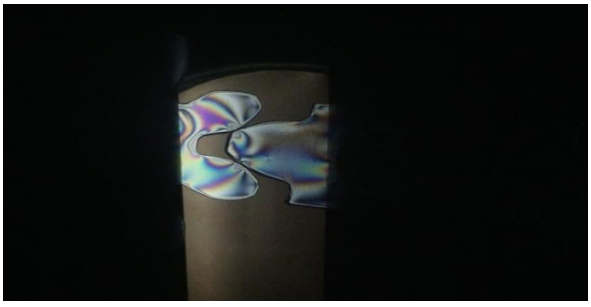

Fig.24 Fringe pattern

The stresses generated are within the maximum permissible limit of material i.e. 250MPa (Table 2). The deformation is reduced from 0.0102 mm to 0.0079 mm. The best root fillet radius observed is 1.5mm in which equivalent stress generated 140.1MPa and deformation 0.00792mm. FEA is a good tool for analysing contact problems, predict stresses & deformations in system and results of stresses obtained from photoelastic analysis are in good agreement with the results obtained from finite technique. The error observes while comparing results can be because of involvement of human being.

References

1. B.J. Hamrock, R.S. Steven, O.J. BoFundame ntals of machine elements (second ed.), McGraw-Hill, Chicago (2005)
2. A. Kawalec, J. Wiktor, D. CeglarekCompara tive analysis of tooth-root strength using ISO and AGMA standards in spur and helical gears with fem-based verification J. Mech. Des., Trans. ASME, 128 (5) (2006), pp. 1141-1158
3. Sankpal A. M and M. M. Mirza, "Contact stress analysis of spur gear by photoelastic technique and finite element analysis", International journal on theoretical and applied research in mechanical engineering (IJTARME), (2014) ISSN: 2319-3182, Volume -3, Issue-2,
4. Rahate H. P and Marne R. A. "Contact stress analysis of composite spur gear using photo-stress method and finite element analysis" (IRJET) (2016) ISSN: 2395 -0056 Volume: 03 Issue: 07
5. Naik K. N. and Dhananjay R. D. "Static analysis of bending stresses on spur gear tooth profile by using finite element analysis and photo elastic technique "International journal of current engineering and technology (IJCET) (2016) ISSN: 2277 – 4106
6. M. Rameshkumar, G. V and P. Shivkumar, "Finite element analysis of high contact ratio gear" AGMA Technical paper, (2010)ISBN: 978-1-55589-981-3
7. Patil S S., Saravanan K, Ivana A and Azmi A W, "Contact stress analysis of helical gear pair including frictional coefficient", International journal of mechanical sciences.85 (2014)ISSN: 205–211
8. ISO 6336-2:2003. "Calculation of load capacity of spur and helical gears, Part 2: Calculation of surface durability (pitting)".
9. ISO 6336-3:2003. "Calculation of load capacity of spur and helical gears, Part 3: Calculation of tooth bending strength".
10. Karaveer V, Ashish M and T. Preman R. J, "Modeling and finite element analysis of spur gear", International journal of current engineering and technology, (IJCET) (2013) ISSN: 2277-4106
11. ShindeS.P. ,Nikam A.A., Mulla T.S., "Static analysis of spur gear using finite element analysis", IOSR journal of Mechanical and Civil Engineering, ISSN: 2278-1684
12. Sankar S., Sundar Raj M., Nataraj M., "Profile Modification for Increasing the Tooth Strength in Spur Gear Using CAD", Scientific Research Journal, (2010) ISSN:1947-3931.
13. Rameshkumar M., Shivkumar P., Sundaresh and S. Gopiath K., "Load sharing analysis of high contact ratio spur gears in military tracked vehicle applications", gear technology, July 2010.
14. K. Mao, "Gear teeth contact analysis and its application in the reduction of fatigue wear", Wear 262 (2007), ISSN 1281–1288
15. R.S. KHURMI and J.K. GUPTA, Machine Design, Ist Edition, Eurasia Publishing House (Pvt.) Ltd, Ram Nagar, New Delhi-110 055 (2005), 1043-1044.

How to cite this article:

Yatih Nupur. 2020. Optimization of Spur Gear Design with Different Root Fillet Profile. *Int.J.Curr.Microbiol.App.Sci.* 9(10): 2327-2338. doi: https://doi.org/10.20546/ijcmas.2020.910.280